

Mechanism and Stereochemistry of Rhodium-Catalyzed [5 + 2 + 1] Cycloaddition of Ene–Vinylcyclopropanes and Carbon Monoxide Revealed by Visual Kinetic Analysis and Quantum Chemical Calculations

Yi Wang, Wei Liao, Yuanyuan Wang, Lei Jiao, and Zhi-Xiang Yu*



Cite This: <https://doi.org/10.1021/jacs.1c11030>



Read Online

ACCESS |



Metrics & More

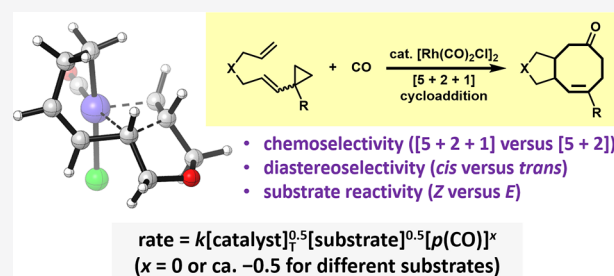


Article Recommendations



Supporting Information

ABSTRACT: Previously, we developed a rhodium-catalyzed [5 + 2 + 1] cycloaddition of ene–vinylcyclopropanes (ene–VCPs) and carbon monoxide to synthesize eight-membered carbocycles. The efficiency of this reaction can be appreciated from its application in the synthesis of several natural products. Herein we report the results of a 15-year investigation into the mechanism of the [5 + 2 + 1] cycloaddition by applying visual kinetic analysis and high-level quantum chemical calculations at the DLPNO-CCSD(T)//BMK level. According to the kinetic measurements, the resting state of the catalyst possesses a dimeric structure (with two rhodium centers) whereas the active catalytic species is monomeric (with one rhodium center). The catalytic cycle consists of cyclopropane cleavage (the turnover-limiting step), alkene insertion, CO insertion, reductive elimination, and catalyst transfer steps. Other reaction pathways have also been considered but then have been ruled out. The steric origin of the diastereoselectivity (*cis* versus *trans*) was revealed by comparing the alkene insertion transition states. In addition, how the double-bond configuration of the VCPs (*Z* versus *E*) affects the substrate reactivity and the origins of chemoselectivity ([5 + 2 + 1] versus [5 + 2]) were also investigated. The present study will provide assistance in understanding other carbonylative annulations catalyzed by transition metals.

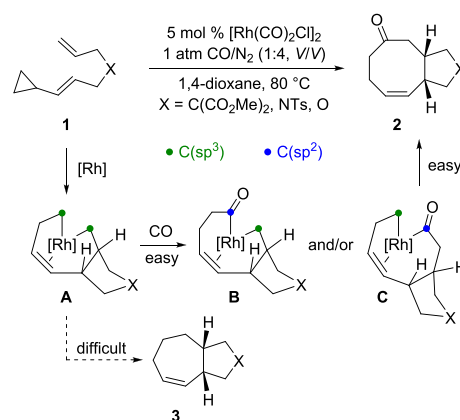


INTRODUCTION

Eight-membered carbocycles are widely found in natural products, pharmaceuticals, and fragrances.^{1–6} Yet due to the unfavorable enthalpic and entropic effects associated with the ring-closure processes,^{7,8} only a limited number of strategies and tactics have been applied to the construction of eight-membered carbocycles.^{9–22} Among them, transition-metal-catalyzed cycloadditions have been proven to be an efficient and atom-economical way to synthesize eight-membered carbocycles with different substitution patterns and stereostructures.^{16–22}

In 2007, we designed a rhodium-catalyzed two-component [5 + 2 + 1] cycloaddition of ene–vinylcyclopropanes (ene–VCPs) **1** and CO (Scheme 1).^{23–27} Our hypothesis was that, under a CO atmosphere, Wender's eight-membered rhoda-cycle intermediate **A** may undergo CO insertion and then C(sp²)–C(sp³) reductive elimination to furnish the [5 + 2 + 1] cycloadduct **2** instead of giving [5 + 2] cycloadduct **3** via the sluggish C(sp³)–C(sp³) reductive elimination.^{28–35} This hypothesis was supported by density functional theory (DFT) calculations and later verified by experiments. The [5 + 2 + 1] cycloaddition of ene–VCPs and CO provides efficient access to cyclooctenones with good to excellent yields. Our group has successfully applied this reaction to the synthesis of several

Scheme 1. Computationally Designed Rhodium-Catalyzed [5 + 2 + 1] Cycloaddition of Ene–VCPs and CO



Received: October 19, 2021

natural products containing eight-membered carbocycles or triquinane skeletons (generated by transannular reactions of the 5,8-fused cycloadducts).^{36–41} Applications of the $[5 + 2 + 1]$ cycloaddition are still ongoing in our laboratory.⁴²

Though we had computed several key steps of the competing $[5 + 2 + 1]$ and $[5 + 2]$ cycloadditions (starting from intermediate A; X = CH₂) in our previous work,²³ follow-up mechanistic studies are essential for (1) understanding the full catalytic cycle of the $[5 + 2 + 1]$ cycloaddition, (2) improving the selectivity of the target reaction, (3) designing new reactions and catalysts, etc.

However, theoretical studies on transition-metal-catalyzed multistep reactions are challenging.^{43–50} It is difficult to select an appropriate computational method that is accurate in describing all of the elementary steps, such as ligand association and dissociation, oxidative addition, reductive elimination, and migratory insertion. As a result, considerable ambiguity in the key mechanistic information cannot be avoided, preventing a full and deep understanding of the reaction mechanism. In addition, identifying the active catalytic species and understanding how they are generated from the precatalysts are also difficult tasks.

Presented here is the final stretch of a 15-year odyssey toward understanding the mechanism of the rhodium-catalyzed $[5 + 2 + 1]$ cycloaddition of ene-VCPs and CO. During the research, we found that different computational methods provided inconsistent conclusions on many important issues, such as the nature of the turnover-limiting step and the origins of chemo- and stereoselectivities. Fortunately, the recent development of hardware and software, especially accurate and efficient computational methods, has enabled us to routinely perform high-level quantum chemical calculations on the real reaction systems (up to 55 atoms in this work) with reasonable accuracy.

We performed a detailed benchmark study against CCSD(T)/def2-TZVPP//TPSS/def2-TZVPP calculations (see the Supporting Information for details),^{51–54} finding that the BMK functional⁵⁵ is superior to the other 23 functionals we tested. On the basis of the BMK-optimized structures, energy refinements using the state of the art DLPNO-CCSD(T) method (with tight thresholds, the accuracy relative to CCSD(T) calculations is expected to be ca. 1 kcal/mol) allowed us to understand the $[5 + 2 + 1]$ cycloaddition both qualitatively and quantitatively.^{56–58} We have also established the rate law directly from concentration profiles using Burés' visual kinetic analysis,^{59–61} which requires fewer experiments but provides more mechanistic information in comparison to the typical method of initial rates. It is worth mentioning that not only does the current study provide mechanistic insights into the $[5 + 2 + 1]$ cycloaddition but also the research paradigm present in this work will inspire mechanistic studies on other rhodium-catalyzed reactions,⁶² especially multi-component carbonylative annulations: e.g., the Pauson–Khand reaction.^{63–66}

RESULTS AND DISCUSSION

Visual Kinetic Analysis. Since the first mechanistic study on $[\text{Rh}(\text{CO})_2\text{Cl}]_2$ -catalyzed intermolecular $[5 + 2]$ cycloaddition⁶⁷ of VCPs and alkynes by Yu, Wender, and Houk in 2004,⁶⁸ monomeric rhodium complexes have been regarded as the catalytic species in Rh–VCP chemistry. These complexes were proposed to be generated from the dissociation of the dimeric catalyst, $[\text{Rh}(\text{CO})_2\text{Cl}]_2$. Though this proposal has

been widely applied to address the issues of mechanism and selectivities for rhodium-catalyzed cycloadditions of VCPs, such as $[5 + 2]$,^{69–75} $[3 + 2 + 1]$,⁷⁶ formal $[5 + 1]/[2 + 2 + 1]$,⁷⁷ and $[5 + 1 + 2 + 1]$ ^{78,79} cycloadditions, no experiments were carried out to verify such a hypothesis.

To investigate the nuclearity of the catalytic species (mono- versus dinuclear), we performed visual kinetic analysis to determine the reaction order in the catalyst, ene–VCPs, and CO. The reaction of trifluoromethylated substrate **1a** (Figure 1) was monitored by ¹⁹F NMR spectroscopy and then

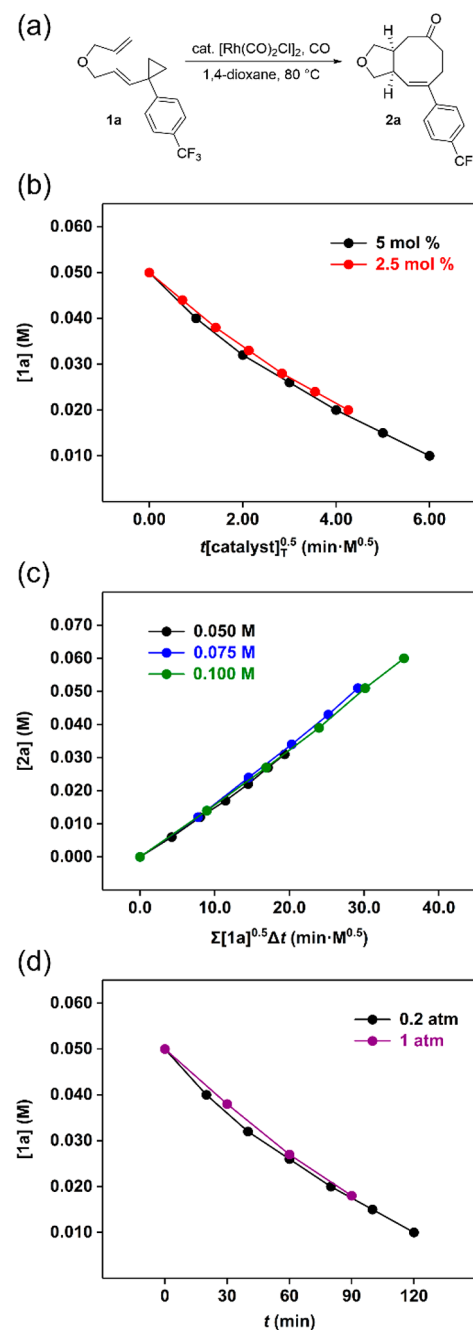
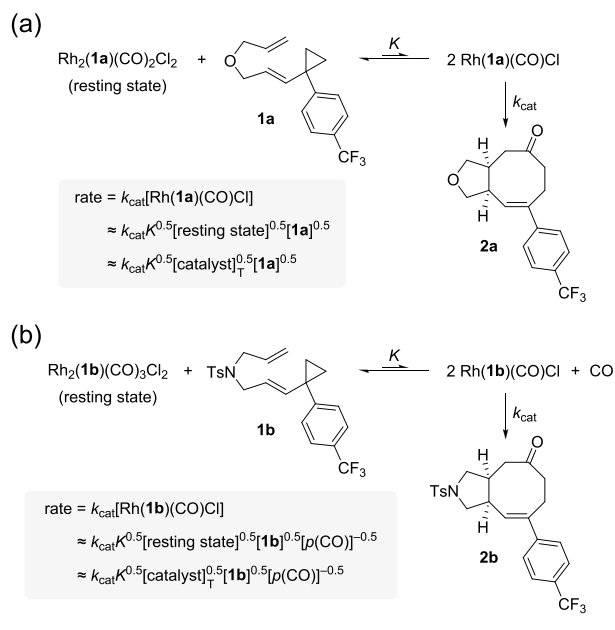


Figure 1. (a) Visual kinetic analysis on the cycloaddition of substrate **1a** and CO. Reaction conditions: (b) **1a** (0.050 M), $[\text{Rh}(\text{CO})_2\text{Cl}]_2$ (5, 2.5 mol %), CO (0.2 atm), 1,4-dioxane, 80 °C; (c) **1a** (0.050, 0.075, 0.100 M), $[\text{Rh}(\text{CO})_2\text{Cl}]_2$ (2.5 mM), CO (0.2 atm), 1,4-dioxane, 80 °C; (d) **1a** (0.050 M), $[\text{Rh}(\text{CO})_2\text{Cl}]_2$ (5 mol %), CO (0.2, 1 atm), 1,4-dioxane, 80 °C.

analyzed by the normalized time scale method⁵⁹ and variable time normalization analysis.⁶⁰ Interestingly, we found that the [5 + 2 + 1] cycloaddition is half order in both $[\text{Rh}(\text{CO})_2\text{Cl}]_2$ and **1a**. The half order in catalyst (Figure 1b; $[\text{catalyst}]_T$ is the total concentration of catalyst added) suggests that there exists an equilibrium between a dimeric off-cycle resting state and a monomeric catalytic species (Scheme 2a). Considering the half

Scheme 2. Equilibrium between Dimeric Resting State and Monomeric Catalytic Species



order in substrate **1a** (Figure 1c), we propose that the resting state contains two rhodium centers and one substrate

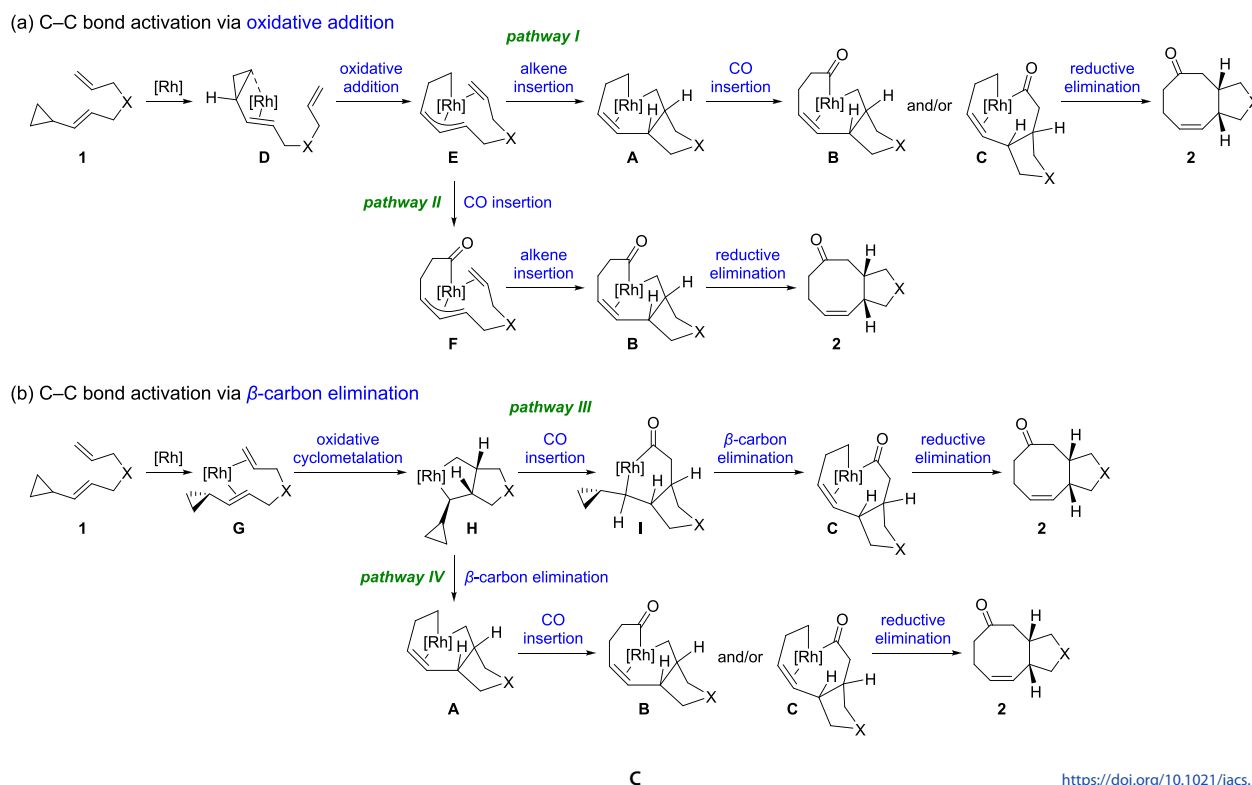
molecule, whereas the catalytic species includes one rhodium center and one substrate. The nearly identical kinetic profiles under 0.2 and 1 atm reveal the zeroth order in CO (Figure 1d), indicating that the number of CO ligands in the resting state is twice as many as that in the turnover-limiting transition state. Further quantum chemical studies reveal that the turnover-limiting transition state only contains one CO ligand (*vide infra*).

To test the generality of these results, we performed a visual kinetic analysis on the reaction of nitrogen-tethered substrate **1b** (Scheme 2b). Though the half order in catalyst and substrate holds, the order in CO changes to ca. negative half (see the Supporting Information for details). We suggest that the composition of the resting state could be different from that of substrate **1a**. For the nitrogen-tethered substrate, one CO molecule is released during the dimer dissociation, resulting in the negative effect of CO pressure on the reaction rate.^{80,81}

According to the kinetic measurements, we suggest that the catalytic species of the [5 + 2 + 1] cycloaddition should be monomeric, whereas the resting state contains two rhodium atoms, two chlorides, one ene-VCP moiety, and two or three CO ligands. However, the exact composition of the resting state is unclear at this stage. Especially, the participation of the solvent molecule, 1,4-dioxane,⁸² cannot be excluded due to its silent behavior during kinetic measurements.

Possible Reaction Pathways. Four possible reaction pathways, namely pathways I–IV, are proposed for the rhodium-catalyzed [5 + 2 + 1] cycloaddition of ene-VCPs and CO (Scheme 3). In pathways I and II, the C–C bond activation of the cyclopropane moiety proceeds through an oxidative addition process (Scheme 3a). In pathway I, alkene inserts into the Rh–C bond first, whereas CO insertion takes place prior to alkene insertion in pathway II

Scheme 3. Possible Reaction Pathways



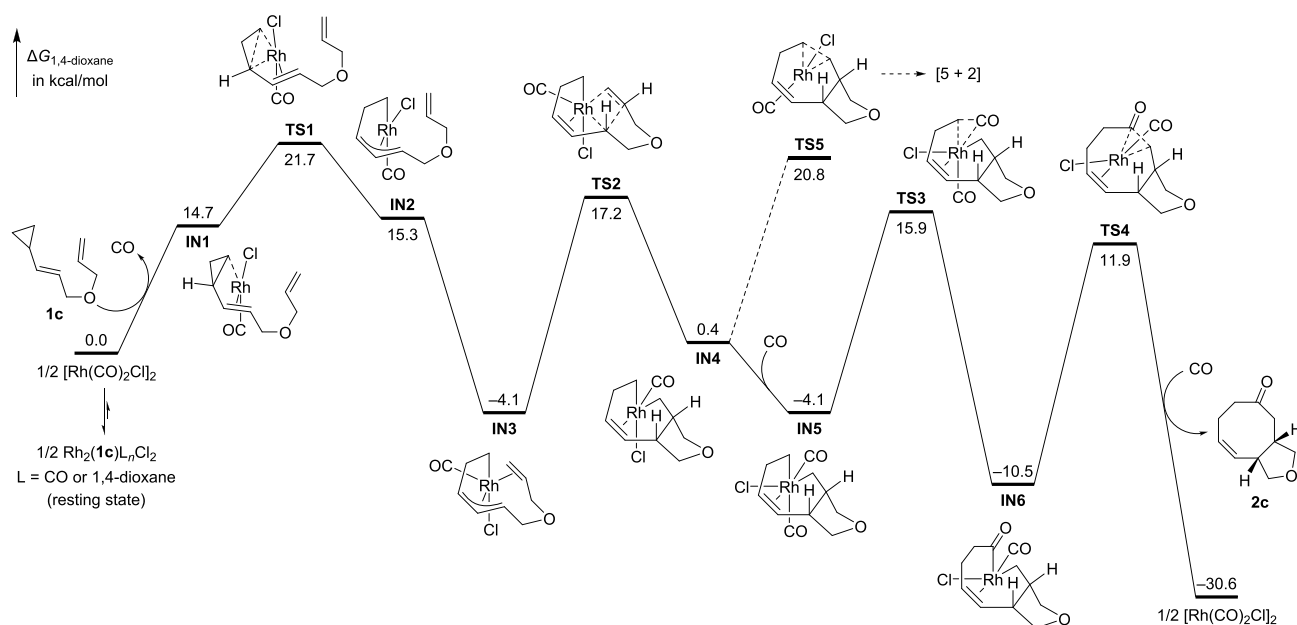


Figure 2. Gibbs energy profile for pathway I, computed at the DLPNO-CCSD(T)/def2-TZVPP:SMD(1,4-dioxane)//BMK/def2-SVP level. The equilibrium between $[\text{Rh}(\text{CO})_2\text{Cl}]_2$ and the resting state is depicted schematically.

(it can be referred to as the $[5 + 1 + 2]$ cycloaddition pathway). In pathways III and IV, the cyclopropane cleavage is achieved by β -carbon elimination (Scheme 3b). Pathways III and IV both start from the oxidative cyclometalation but differ in the sequence of CO insertion and β -carbon elimination. In what follows, all of these pathways will be discussed with the aid of quantum chemical calculations.

We utilized ene-VCP **1c** ($X = \text{O}$), a real substrate employed in our previous experiments,²³ as the model substrate for computations. For each transition state, we have considered the variation of the number of CO ligands as well as the configuration of the rhodium center. Only the most favored transition states are discussed unless otherwise specified.

Pathway I. As was mentioned above, though we have proved that the resting state consists of two rhodium centers and one substrate, its exact composition is unclear at the current stage and may vary from one substrate to another. Considering that the resting state is an off-cycle species that would not affect the discussion of the catalytic cycle and selectivities, we did not spend time and computational resources on the resting state. Instead, we treated $[\text{Rh}(\text{CO})_2\text{Cl}]_2$ as the starting point of the Gibbs energy profile.

As depicted in Figure 2, the catalytic cycle starts from the complexation of substrate **1c** to the rhodium center, giving a 16-electron intermediate, **IN1**. Then, cyclopropane cleavage takes place via oxidative addition transition state **TS1**, in which the terminal alkene does not coordinate to the metal center. The complexation of the terminal alkene or an additional CO ligand cannot accelerate the cyclopropane cleavage process (see the Supporting Information for details).

After the oxidative addition, 16-electron intermediate **IN2** undergoes an intramolecular alkene complexation to form an 18-electron intermediate, **IN3**, which then triggers the alkene insertion via **TS2** with an activation Gibbs energy of 21.3 kcal/mol. The resulting rhodacyclooctene **IN4** proceeds through the complexation and insertion of CO (**IN4** \rightarrow **IN5** \rightarrow **TS3** \rightarrow **IN6**); we assume that there exists an equilibrium between **IN4** and **IN5**, see the Supporting Information for details) to afford

rhodacyclononene **IN6**. Finally, **IN6** undergoes reductive elimination via **TS4** to deliver the $[5 + 2 + 1]$ cycloadduct **2c**. Considering that **TS1** > **TS2** > **TS3** > **TS4** in terms of Gibbs energies, we conclude that the oxidative addition, alkene insertion, CO insertion, and reductive elimination steps are all irreversible.

Pathway II. This pathway consists of oxidative addition, CO insertion, alkene insertion, and reductive elimination (Scheme 3a). It differs from pathway I in the sequence of CO insertion and alkene insertion. In pathway II, instead of alkene complexation and insertion (via **IN2** \rightarrow **IN3** \rightarrow **TS2** \rightarrow **IN4** in Figure 2), **IN2** undergoes CO complexation to generate an 18-electron intermediate, **IN7**, followed by CO insertion via **TS6** (Figure 3). Considering that the alkene insertion transition state **TS2** in pathway I is favored over the CO insertion transition state **TS6** in pathway II by 11.2 kcal/mol, we can exclude the possibility of pathway II for further

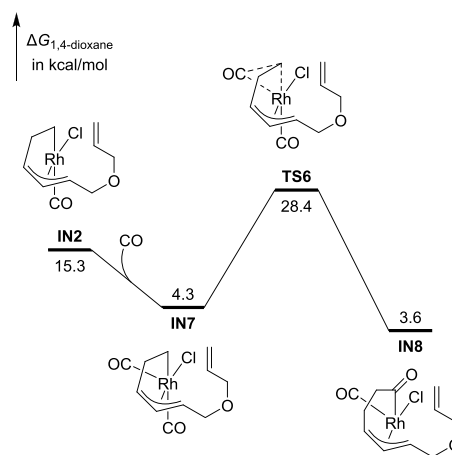


Figure 3. CO complexation and insertion in pathway II, computed at the DLPNO-CCSD(T)/def2-TZVPP:SMD(1,4-dioxane)//BMK/def2-SVP level.

consideration (see the Supporting Information for more discussion).

Pathways III and IV. Pathways III and IV both start from oxidative cyclometalation (Scheme 3b). Therefore, we computed the oxidative cyclometalation process of substrate **1c** to investigate whether pathways III and IV are favored over the others (Figure 4). $[\text{Rh}(\text{CO})_2\text{Cl}]_2$ reacts with **1c** to form an

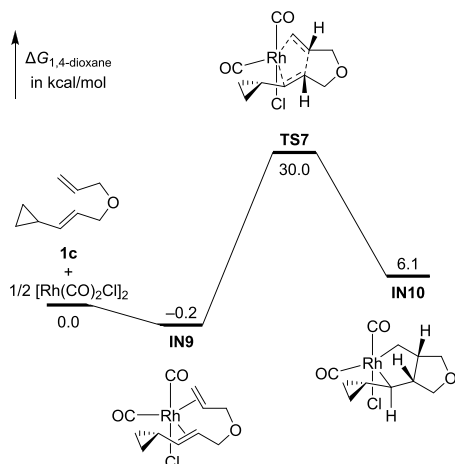


Figure 4. Gibbs energy profile for oxidative cyclometalation, computed at the DLPNO-CCSD(T)/def2-TZVPP:SMD(1,4-dioxane)//BMK/def2-SVP level.

18-electron intermediate, **IN9**, followed by oxidative cyclometalation via **TS7** with an activation Gibbs energy of 30.2 kcal/mol. Considering that **TS7** is more energy-demanding than **TS1** in pathway I by 8.3 kcal/mol, we can safely rule out pathways III and IV.

Summary of the Reaction Mechanism. According to these computational results, we suggest that pathway I is the most favored reaction pathway. The activation Gibbs energies of oxidative addition, alkene insertion, CO insertion, and reductive elimination are 21.9 (calculated from **IN9** to **TS1**), 21.3, 20.0, and 22.4 kcal/mol, respectively. On consideration that the resting state has not been computed, the Gibbs energy barrier of the oxidative addition is certainly underestimated and thus should be larger than the computed barrier. After taking the rate law into consideration (the reaction is half order in both catalyst and substrate), we suggest that the C–C bond activation should be the turnover-limiting step. As summarized in Figure 5, the mechanism of the rhodium-catalyzed [5 + 2 + 1] cycloaddition is composed of dimeric resting state dissociation, oxidative addition, alkene insertion, CO insertion, reductive elimination, and catalyst transfer.

Though the reductive elimination of **B** and **C** leads to the same [5 + 2 + 1] cycloadduct, the preference for the generation of **B** or **C** is substrate-dependent. For substrate **1c**, the formation of intermediate **B** ($X = \text{O}$; $[\text{Rh}] = \text{Rh}(\text{CO})\text{Cl}$) via **TS3** is favored over CO insertion into the other Rh–C bond (see the Supporting Information for details). In fact, the generation of **C** is also possible for some substrates (see later discussion in Table 1). Therefore, intermediates **B** and **C** are both depicted in Figure 5.

Discussion of the Substrate Reactivity. *Experimental Observations.* During our synthesis of asterisca-3(15),6-diene, pentalenene, and hirsutene, we noticed that substrate (**Z**)-**1d** reacted more slowly than its *E* isomer (Figure 6a).^{37,38} To further confirm these observations, we reinvestigated the

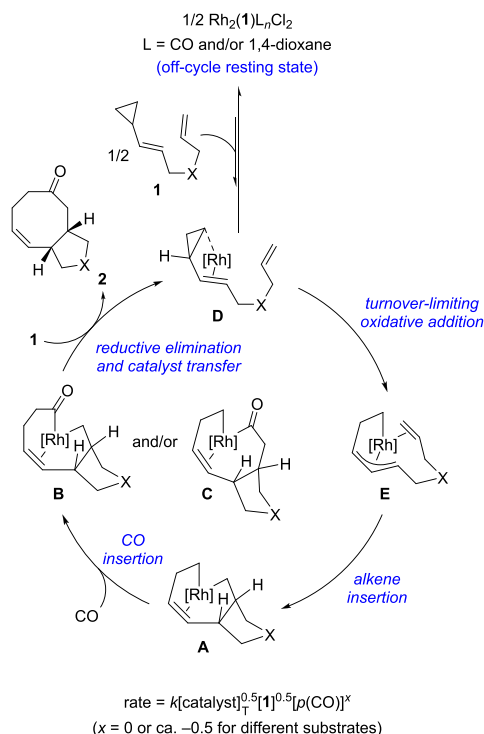


Figure 5. Reaction mechanism supported by kinetic measurements and quantum chemical calculations in which $[\text{Rh}]$ is monomeric.

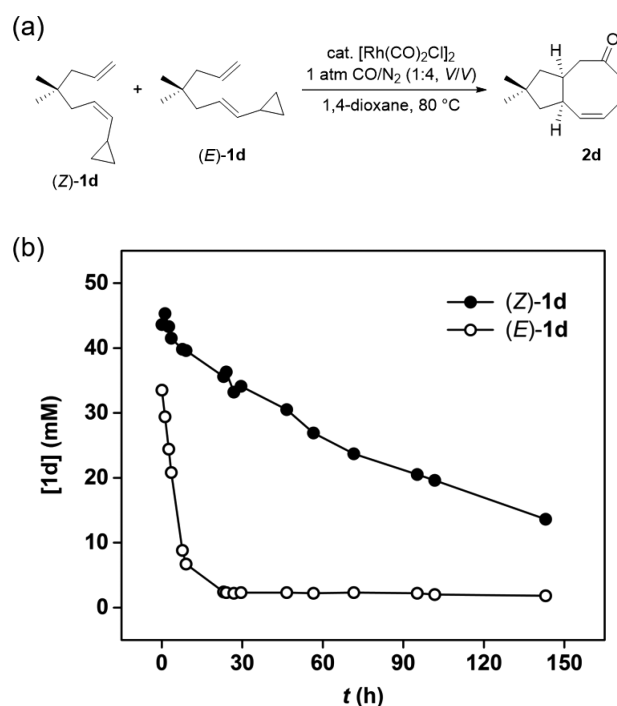


Figure 6. Kinetic profile for the reaction of a mixture of (*Z*)- and (*E*)-**1d**. Reaction conditions: $[(\text{Z})\text{-1d}]_0 = 0.0436 \text{ M}$, $[(\text{E})\text{-1d}]_0 = 0.0335 \text{ M}$, $[\text{catalyst}]_T = 3.6 \text{ mM}$, CO (0.2 atm), 1,4-dioxane, 80 °C.

reaction of a 1.3:1 mixture of (*Z*)- and (*E*)-**1d** and monitored its kinetic profile by gas chromatography (GC). As is clearly depicted in Figure 6b, substrate (*Z*)-**1d** indeed reacts much more slowly than its *E* counterpart.

Quantum Chemical Calculations. To understand how the double-bond configuration of the VCPs (*Z* versus *E*) affects

the substrate reactivity, we computed the turnover-limiting cyclopropane cleavage of both *Z* and *E* substrates (Figure 7).

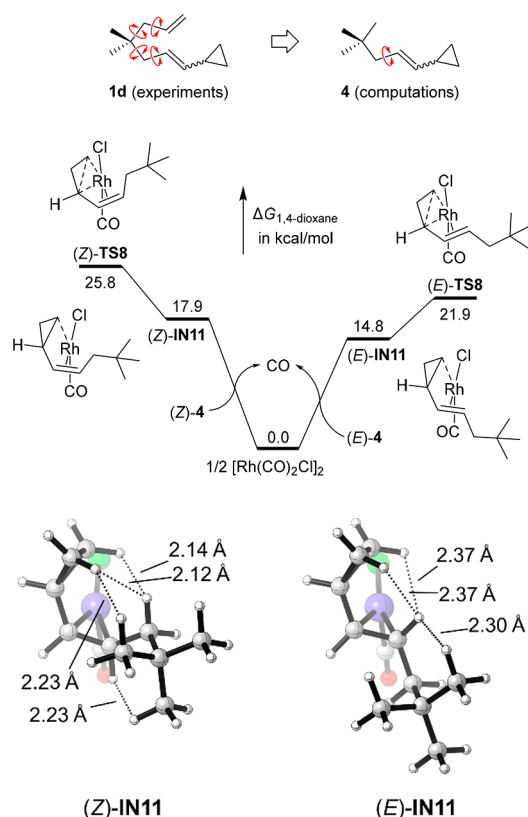
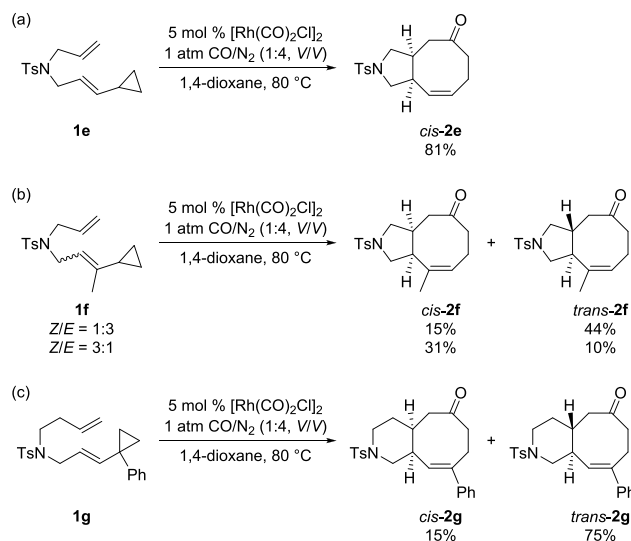


Figure 7. Gibbs energy profile for the cyclopropane cleavage of model substrates (*Z*)- and (*E*)-**4**, computed at the DLPNO-CCSD(T)/def2-TZVPP:SMD(1,4-dioxane)//BMK/def2-SVP level. Color scheme: H, white; C, gray; O, red; Cl, green; Rh, violet.

To simplify the computations, we replaced the allyl groups in (*Z*)- and (*E*)-**1d** by methyl groups, resulting in the model substrates (*Z*)- and (*E*)-**4**, respectively. Despite similar activation Gibbs energies for the cyclopropane cleavage step (7.1 kcal/mol for (*E*)-IN11 versus 7.9 kcal/mol for (*Z*)-IN11), the reaction of the *E* isomer is predicted to be significantly easier than that of the *Z* isomer ($\Delta\Delta G^\ddagger = 3.9$ kcal/mol), which nicely reproduces the experimental observations. We attribute the different reactivities of *Z* and *E* substrates to the different thermodynamic stabilities of intermediates (*Z*)- and (*E*)-IN11. As shown in Figure 7, the steric repulsions in (*Z*)-IN11 are more severe than those in its *E* counterpart. Therefore, in comparison with the *E* substrate, the *Z* substrate requires a higher preorganization energy to reach the reactive intermediate, leading to a slower reaction rate.

Discussion of the Stereochemistry. *Experimental Observations.* Our [5 + 2 + 1] cycloaddition generates two new stereogenic centers at the bridgehead carbons. In most cases, the reaction furnishes *cis*-fused bicycles diastereoselectively.²³ For example, the NTs-tethered substrate **1e** with an *E* configuration gave the *cis*-5,8-fused bicyclic product *cis*-**2e** in 81% yield (Scheme 4a). Surprisingly, when a methyl group was introduced into the α position of the VCP moiety, *trans*-5,8-fused bicycle *trans*-**2f** became the major product (Scheme 4b). Changing the double-bond configuration of the VCP from *E* to *Z* resulted in the reversal of the diastereoselectivity from *trans* back to *cis* (Scheme 4b). Finally, the [5 + 2 + 1] cycloaddition

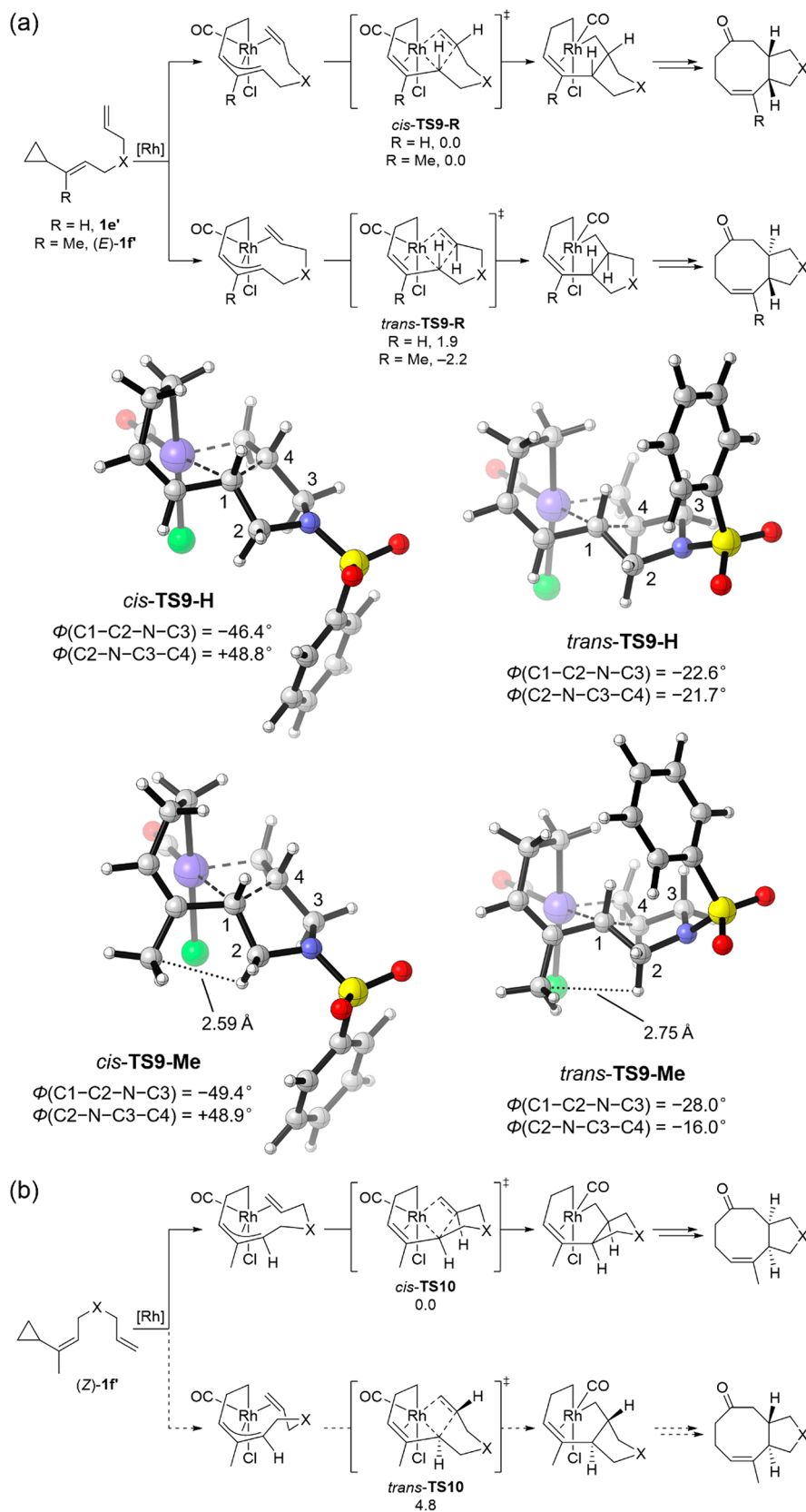
Scheme 4. Stereochemistry of the [5 + 2 + 1] Cycloaddition



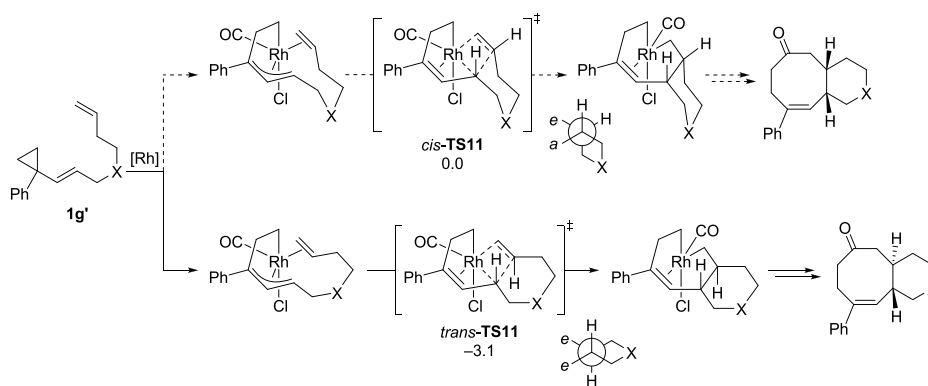
of elongated substrate **1g** gave *trans*-6,8-fused bicycle *trans*-**2g** as the major product (Scheme 4c).

Quantum Chemical Calculations. As was mentioned above, the alkene insertion step is irreversible and thus determines the stereochemistry.⁸³ Considering that the internal rotation of the methyl group on the tosyl group may lead to slow convergence during geometry optimizations, we replaced all the tosyl groups by benzenesulfonyl groups to simplify the computations. For the model substrate **1e'**, the *cis*-insertion transition state *cis*-TS9-H is favored over *trans*-TS9-H by 1.9 kcal/mol (Scheme 5a), suggesting that the *cis*-5,8-fused cycloadduct should be obtained as the major product, which nicely agrees with the experiments (Scheme 4a). We attribute such a diastereoselectivity to the different ring strains of the forming five-membered rings in the transition states. In *cis*-TS9-H, the dihedral angles $\Phi(C1-C2-N-C3)$ and $\Phi(C2-N-C3-C4)$ are -46.4 and $+48.8^\circ$, respectively. The corresponding values in *trans*-TS9-H are much smaller (-22.6 and -21.7°), indicating a larger torsional strain in the *trans*-insertion transition state. For the model substrate (*E*)-**1f'**, due to the introduction of a methyl group, an additional transannular strain between the methyl group and one hydrogen atom attached to C2 arises (Scheme 5a). The nonbonding C...H distances in *cis*- and *trans*-TS9-Me are 2.59 and 2.75 Å, respectively, suggesting that the transannular strain in the *cis*-insertion transition state is more severe than that in the *trans*-insertion transition state. As a result, *trans*-TS9-Me is predicted to be favored over *cis*-TS9-Me by 2.2 kcal/mol, which is in good agreement with the experimental observations (Scheme 4b). In contrast, for the *Z* isomer (*Z*)-**1f'**, because the methyl group is far away from the tether, there is no transannular strain originating from the methyl group. Therefore, in this case, the *cis*-insertion transition state *cis*-TS10 with a smaller torsional strain becomes favored again (Scheme 5b).

Then, we considered the elongated model substrate **1g'** (Scheme 6). In the *cis*-insertion transition state *cis*-TS11, the forming six-membered ring is fused to the rhodacycle through an equatorial bond and an axial bond, resulting in additional gauche interactions, which are absent in its *trans* counterpart (*trans*-TS11), whose rings are connected by two equatorial bonds. Thus, *trans* insertion is predicted to be favored in this

Scheme 5. Stereochemistry of 5,8-Fused Bicycle Formation^a

^aDefinition: X = NSO₂Ph. Relative Gibbs energies are reported in kcal/mol, computed at the DLPNO-CCSD(T)/def2-TZVPP:SMD(1,4-dioxane)//BMK/def2-SVP level. Color scheme: H, white; C, gray; N, blue; O, red; S, yellow; Cl, green; Rh, violet.

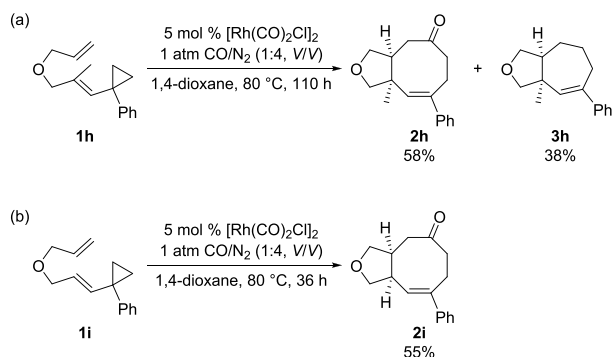
Scheme 6. Stereochemistry of 6,8-Fused Bicycle Formation^a

^aDefinitions: X = NSO₂Ph. e = equatorial, a = axial. Relative Gibbs energies are reported in kcal/mol, computed at the DLPNO-CCSD(T)/def2-TZVPP:SMD(1,4-dioxane)//BMK/def2-SVP level.

case, which qualitatively matches our experiments (Scheme 4c).

Discussion of the Chemoselectivity. Experimental Observations. As was mentioned in the Introduction, our design was based on the hypothesis that [5 + 2] cycloaddition of ene-VCPs is difficult due to the sluggish C(sp³)-C(sp³) reductive elimination. For the model substrate **1c**, the C(sp³)-C(sp³) reductive elimination transition state **TS5** is disfavored over the CO insertion transition state **TS3** by 4.9 kcal/mol (Figure 2; see the Supporting Information for details), suggesting that only the [5 + 2 + 1] cycloadduct **2c** will be generated. Admittedly, during the past decade, dozens of ene-VCP substrates have been treated with [Rh(CO)₂Cl]₂ under a CO atmosphere and almost all the tested substrates led to the [5 + 2 + 1] cycloadducts rather than the [5 + 2] cycloadducts. One of the exceptions is substrate **1h** with a methyl group at the β position of the VCP moiety, which gave both the [5 + 2 + 1] and [5 + 2] cycloadducts under the standard conditions (Scheme 7a).⁴² In contrast, substrate **1i**, which does not have the β-methyl group, only furnished the [5 + 2 + 1] cycloadduct **2i** (Scheme 7b).

Scheme 7. [5 + 2 + 1] versus [5 + 2] Cycloadditions

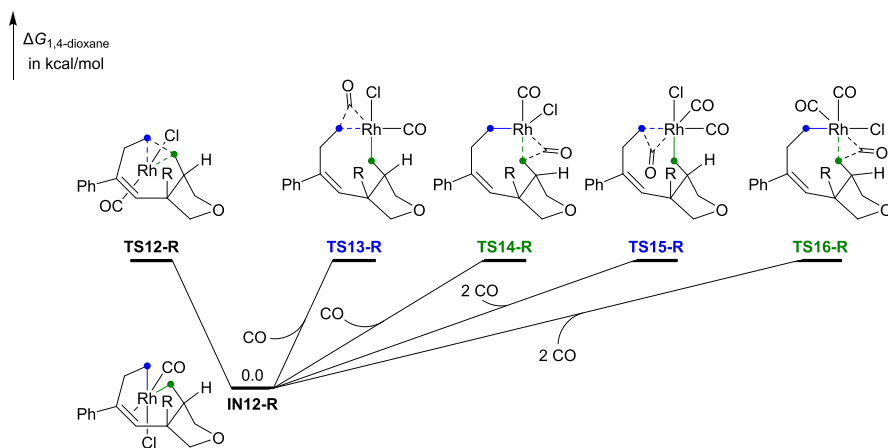


Quantum Chemical Calculations. To understand the competition between [5 + 2] and [5 + 2 + 1] cycloadditions, we computed the C(sp³)-C(sp³) reductive elimination transition state **TS12-R** (R = Me for **1h**; R = H for **1i**) in the [5 + 2] cycloaddition and several CO insertion transition states in the [5 + 2 + 1] cycloaddition (Table 1). For CO insertion transition states with two CO ligands, **TS13-R** and **TS14-R** are the most favored transition states for insertion into

two distinct Rh-C(sp³) bonds, respectively. **TS15-R** and **TS16-R** are the most favored CO insertion transition states with three CO ligands. Considering that the CO insertion is irreversible (*vide supra*), we do not discuss here the following C(sp²)-C(sp³) reductive elimination to give [5 + 2 + 1] cycloadducts.⁸⁴

For substrate **1h**, the most favored CO insertion transition state **TS16-Me** is predicted to be slightly favored over the C(sp³)-C(sp³) reductive elimination transition state **TS12-Me**, indicating that both [5 + 2 + 1] and [5 + 2] cycloadducts should be formed. For substrate **1i**, the most favored CO insertion transition state **TS15-H** is favored over the C(sp³)-C(sp³) reductive elimination transition state **TS12-H** by 2.1 kcal/mol, suggesting that the [5 + 2 + 1] cycloadduct **2i** should be generated predominantly. These results agree with our experiments (Scheme 7). To exemplify how the β-methyl group affects the chemoselectivity, we compared the 3D structures of **TS15-Me** and **TS15-H** (Figure 8). In comparison with **TS15-H**, **TS15-Me** possesses an additional transannular strain caused by the methyl group with a nonbonding C...H distance of 2.57 Å, resulting in the sluggish CO insertion for substrate **1h**.

Experimental Verification and Reaction Optimization. Our computations suggest that the competing **TS12-Me** and **TS16-Me** have one and three CO ligands, respectively. Therefore, if the pressure of CO increases by a factor of *n*, the ratio of [5 + 2 + 1]/[5 + 2] cycloadducts will increase by a factor of *n*². To verify this hypothesis, we treated substrate **1h** (0.10 mmol) with 5 mol % of [Rh(CO)₂Cl]₂ under 0.1 and 0.2 atm of CO, respectively, finding that the **2h**/**3h** ratio indeed increased by a factor of ca. 4 when the CO pressure was doubled (Table 2, entries 1 and 2; reaction time 16 h). Moreover, under 0.5 and 1 atm of CO, the selectivity toward [5 + 2 + 1] cycloaddition can be further improved (>20/1 **2h**/**3h** in both cases; Table 2, entries 3 and 4; reaction time 16 h). When the reaction was scaled up to 0.60 mmol (reaction time 110 h), the isolated yield of **2h** was improved from 58% (under 0.2 atm of CO) to 74% (under 0.5 atm of CO). We assume that the inefficient mass transfer of CO from the gas phase to the solution phase (the concentration of CO did not reach saturation in time) might have prevented a further increase in the reaction yield.

Table 1. Competition between [5 + 2] and [5 + 2 + 1] Cycloadditions^a

substrate	R	ΔG^\ddagger (kcal/mol)				
		TS12-R	TS13-R	TS14-R	TS15-R	TS16-R
1h	Me	19.4	21.9	21.4	24.4	19.2
1i	H	20.5	19.0	19.2	18.4	18.8

^aComputed at the DLPNO-CCSD(T)/def2-TZVPP:SMD(1,4-dioxane)//BMK/def2-SVP level.

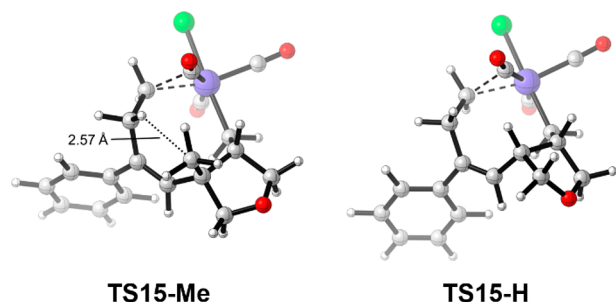


Figure 8. Optimized geometries for TS15-Me and TS15-H, computed at the BMK/def2-SVP level. Color scheme: H, white; C, gray; O, red; Cl, green; Rh, violet.

Table 2. Influence of CO Pressure on the Chemoselectivity^a

entry	<i>x</i>	2h/3h ^b
1	0.1	1.7/1
2	0.2	7.6/1
3	0.5	>20/1
4	1	>20/1

^aReaction conditions: **1h** (0.10 mmol), [Rh(CO)₂Cl]₂ (5 mol %), CO/N₂, 1,4-dioxane, 80 °C, 16 h. ^bDetermined by ¹H NMR analysis.

CONCLUSIONS

The mechanism of the rhodium-catalyzed two component [5 + 2 + 1] cycloaddition of ene-VCPs and CO puzzled us for more than a decade due to the uncertainty of active catalytic species and inconsistent conclusions from different computational methods. These thorny issues have been finally resolved by the combination of visual kinetic analysis and DLPNO-CCSD(T) calculations, showing that the active catalytic species is monomeric whereas the off-cycle catalyst resting state is dimeric. The catalytic cycle consists of cyclopropane

cleavage via oxidative addition (the turnover-limiting step), alkene insertion, CO insertion, reductive elimination, and catalyst transfer. The lower reactivity of (*Z*)-ene-VCPs in comparison to their *E* counterparts is caused by the more severe steric repulsions in the C–C bond activation transition states and their precursors. The diastereoselectivity (*cis* versus *trans*) originates from the tradeoff between different strains in the competing alkene insertion transition states. The chemoselectivity ([5 + 2 + 1] versus [5 + 2]) is determined by the relative ease of the C(sp³)–C(sp³) reductive elimination and the irreversible CO insertion. These mechanistic insights can help chemists understand the present reaction as well as optimize and design other transition-metal-catalyzed cycloadditions.^{85–90}

COMPUTATIONAL METHODS

All DFT calculations were performed with the Gaussian 09 software package.⁹¹ Pruned integration grids with 99 radial shells and 590 angular points per shell were used. Geometry optimizations of all the stationary points were carried out in the gas phase at the BMK⁵⁵/def2-SVP^{52,53} level. Unscaled harmonic frequency calculations at the same level were performed to validate each structure as either a minimum or a transition state and to evaluate its zero-point energy and thermal corrections at 298 K. Quasi-harmonic corrections were applied during the entropy calculations by setting all positive frequencies that were less than 100 cm⁻¹ to 100 cm⁻¹.^{92,93} On the basis of the optimized structures, Gibbs energies of solvation in 1,4-dioxane were computed at the SMD⁹⁴/BMK/def2-SVP level and single-point energy refinements were performed with ORCA 4.2.1^{95,96} at the DLPNO-CCSD(T)^{56,57}/def2-TZVPP^{52,53} level (using the def2-TZVPP/C auxiliary basis set and tight thresholds). All discussed energy differences are based on Gibbs energies in 1,4-dioxane at 298 K. Standard state concentrations of 1.4 mM⁹⁷ and 1.0 M⁹⁸ were used for CO and the other species, respectively. All of the 3D structures were prepared with CYLview.⁹⁹

ASSOCIATED CONTENT

Supporting Information

The Supporting Information is available free of charge at <https://pubs.acs.org/doi/10.1021/jacs.1c11030>.

Experimental procedures, characterization data, NMR spectra, and computational details (PDF)

AUTHOR INFORMATION

Corresponding Author

Zhi-Xiang Yu – Beijing National Laboratory for Molecular Sciences (BNLMS), Key Laboratory of Bioorganic Chemistry and Molecular Engineering of Ministry of Education, College of Chemistry, Peking University, Beijing 100871, People's Republic of China; orcid.org/0000-0003-0939-9727; Email: yuzx@pku.edu.cn

Authors

Yi Wang – Beijing National Laboratory for Molecular Sciences (BNLMS), Key Laboratory of Bioorganic Chemistry and Molecular Engineering of Ministry of Education, College of Chemistry, Peking University, Beijing 100871, People's Republic of China; orcid.org/0000-0001-5762-5958

Wei Liao – Beijing National Laboratory for Molecular Sciences (BNLMS), Key Laboratory of Bioorganic Chemistry and Molecular Engineering of Ministry of Education, College of Chemistry, Peking University, Beijing 100871, People's Republic of China; orcid.org/0000-0002-2896-0025

Yuanyuan Wang – Beijing National Laboratory for Molecular Sciences (BNLMS), Key Laboratory of Bioorganic Chemistry and Molecular Engineering of Ministry of Education, College of Chemistry, Peking University, Beijing 100871, People's Republic of China

Lei Jiao – Beijing National Laboratory for Molecular Sciences (BNLMS), Key Laboratory of Bioorganic Chemistry and Molecular Engineering of Ministry of Education, College of Chemistry, Peking University, Beijing 100871, People's Republic of China; orcid.org/0000-0002-8465-1358

Complete contact information is available at:

<https://pubs.acs.org/10.1021/jacs.1c11030>

Notes

The authors declare no competing financial interest.

ACKNOWLEDGMENTS

This work was supported by the National Natural Science Foundation of China (21933003) and the High-Performance Computing Platform of Peking University. We thank Prof. Chang-Sheng Wang and Dr. Xi-Chan Gao at Liaoning Normal University for allowing us to use their computational resources at the early stages of this work. We also appreciate Ms. Xiu Zhang and Dr. Hui Fu at the Analytical Instrumentation Center of Peking University for their assistance in NMR analysis and Mr. Yi Zhou at Peking University for his assistance in some synthetic experiments.

REFERENCES

- (1) Kavanagh, F.; Hervey, A.; Robbins, W. J. Antibiotic Substances From Basidiomycetes: VIII. *Pleurotus Multilus* (Fr.) Sacc. and *Pleurotus Passekerianus* Pilat. *Proc. Natl. Acad. Sci. U. S. A.* **1951**, *37*, 570–574.
- (2) Wani, M. C.; Taylor, H. L.; Wall, M. E.; Coggon, P.; McPhail, A. T. Plant Antitumor Agents. VI. The Isolation and Structure of Taxol, a Novel Antileukemic and Antitumor Agent from *Taxus brevifolia*. *J. Am. Chem. Soc.* **1971**, *93*, 2325–2327.
- (3) Boden, R. M.; Licciardello, M. Alkyl-4-cyclooctenyl Carbonates and Uses Thereof in Augmenting or Enhancing the Aroma of Perfume Compositions, Colognes and Perfumed Articles. US Patent 4397789, 1983.
- (4) San Feliciano, A.; Barrero, A. F.; Medarde, M.; Miguel del Corral, J. M.; Aramburu, A.; Perales, A.; Fayos, J. Asteriscanolide. A Sesquiterpene Lactone with a New Natural Skeleton. *Tetrahedron Lett.* **1985**, *26*, 2369–2372.
- (5) Uchida, I.; Ando, T.; Fukami, N.; Yoshida, K.; Hashimoto, M.; Tada, T.; Koda, S.; Morimoto, Y. The Structure of Vinigrol, a Novel Diterpenoid with Antihypertensive and Platelet Aggregation-Inhibitory Activities. *J. Org. Chem.* **1987**, *52*, 5292–5293.
- (6) Granier, T.; Bajgrowicz, J. A.; Hanhart, A. Cyclooct-(en-)yl Derivatives for Use as Fragrances. WO Patent 2004/035017 A1, 2004.
- (7) Illuminati, G.; Mandolini, L. Ring Closure Reactions of Bifunctional Chain Molecules. *Acc. Chem. Res.* **1981**, *14*, 95–102.
- (8) Galli, C.; Mandolini, L. The Role of Ring Strain on the Ease of Ring Closure of Bifunctional Chain Molecules. *Eur. J. Org. Chem.* **2000**, *2000*, 3117–3125.
- (9) Petasis, N. A.; Patane, M. A. The Synthesis of Carbocyclic Eight-Membered Rings. *Tetrahedron* **1992**, *48*, 5757–5821.
- (10) Mehta, G.; Singh, V. Progress in the Construction of Cyclooctanoid Systems: New Approaches and Applications to Natural Product Syntheses. *Chem. Rev.* **1999**, *99*, 881–930.
- (11) Maier, M. E. Synthesis of Medium-Sized Rings by the Ring-Closing Metathesis Reaction. *Angew. Chem., Int. Ed.* **2000**, *39*, 2073–2077.
- (12) Michaut, A.; Rodriguez, J. Selective Construction of Carbocyclic Eight-Membered Rings by Ring-Closing Metathesis of Acyclic Precursors. *Angew. Chem., Int. Ed.* **2006**, *45*, 5740–5750.
- (13) Wang, C.; Xi, Z. Metal Mediated Synthesis of Substituted Cyclooctatetraenes. *Chem. Commun.* **2007**, 5119–5133.
- (14) Tori, M.; Mizutani, R. Construction of Eight-Membered Carbocycles with Trisubstituted Double Bonds Using the Ring Closing Metathesis Reaction. *Molecules* **2010**, *15*, 4242–4260.
- (15) Hu, Y.-J.; Li, L.-X.; Han, J.-C.; Min, L.; Li, C.-C. Recent Advances in the Total Synthesis of Natural Products Containing Eight-Membered Carbocycles (2009–2019). *Chem. Rev.* **2020**, *120*, 5910–5953.
- (16) Lautens, M.; Klute, W.; Tam, W. Transition Metal-Mediated Cycloaddition Reactions. *Chem. Rev.* **1996**, *96*, 49–92.
- (17) Ojima, I.; Tzamarioudaki, M.; Li, Z.; Donovan, R. J. Transition Metal-Catalyzed Carbocyclizations in Organic Synthesis. *Chem. Rev.* **1996**, *96*, 635–662.
- (18) Sieburth, S. McN.; Cunard, N. T. The [4 + 4] Cycloaddition and Its Strategic Application in Natural Product Synthesis. *Tetrahedron* **1996**, *52*, 6251–6282.
- (19) Yet, L. Metal-Mediated Synthesis of Medium-Sized Rings. *Chem. Rev.* **2000**, *100*, 2963–3008.
- (20) Inglesby, P. A.; Evans, P. A. Stereoselective Transition Metal-Catalyzed Higher-Order Carbocyclisation Reactions. *Chem. Soc. Rev.* **2010**, *39*, 2791–2805.
- (21) Yu, Z.-X.; Wang, Y.; Wang, Y. Transition-Metal-Catalyzed Cycloadditions for the Synthesis of Eight-Membered Carbocycles. *Chem. - Asian J.* **2010**, *5*, 1072–1088.
- (22) Wang, L.-N.; Yu, Z.-X. Transition-Metal-Catalyzed Cycloadditions for the Synthesis of Eight-Membered Carbocycles: An Update from 2010 to 2020. *Youji Huaxue* **2020**, *40*, 3536–3558.
- (23) Wang, Y.; Wang, J.; Su, J.; Huang, F.; Jiao, L.; Liang, Y.; Yang, D.; Zhang, S.; Wender, P. A.; Yu, Z.-X. A Computationally Designed Rh(I)-Catalyzed Two-Component [5 + 2 + 1] Cycloaddition of Ene-vinylcyclopropanes and CO for the Synthesis of Cyclooctenones. *J. Am. Chem. Soc.* **2007**, *129*, 10060–10061.
- (24) Huang, F.; Yao, Z.-K.; Wang, Y.; Wang, Y.; Zhang, J.; Yu, Z.-X. Rh^I-Catalyzed Two-Component [(5 + 2) + 1] Cycloaddition Approach toward [5–8–5] Ring Systems. *Chem. - Asian J.* **2010**, *5*, 1555–1559.
- (25) Wang, Y.; Yu, Z.-X. Rhodium-Catalyzed [5 + 2 + 1] Cycloaddition of Ene-Vinylcyclopropanes and CO: Reaction Design, Development, Application in Natural Product Synthesis, and

Inspiration for Developing New Reactions for Synthesis of Eight-Membered Carbocycles. *Acc. Chem. Res.* **2015**, *48*, 2288–2296.

(26) Wender, P. A.; Gamber, G. G.; Hubbard, R. D.; Zhang, L. Three-Component Cycloadditions: The First Transition Metal-Catalyzed $[5 + 2 + 1]$ Cycloaddition Reactions. *J. Am. Chem. Soc.* **2002**, *124*, 2876–2877.

(27) Wegner, H. A.; de Meijere, A.; Wender, P. A. Transition Metal-Catalyzed Intermolecular $[5 + 2]$ and $[5 + 2 + 1]$ Cycloadditions of Allenes and Vinylcyclopropanes. *J. Am. Chem. Soc.* **2005**, *127*, 6530–6531.

(28) Wender, P. A.; Husfeld, C. O.; Langkopf, E.; Love, J. A. First Studies of the Transition Metal-Catalyzed $[5 + 2]$ Cycloadditions of Alkenes and Vinylcyclopropanes: Scope and Stereochemistry. *J. Am. Chem. Soc.* **1998**, *120*, 1940–1941.

(29) Wender, P. A.; Husfeld, C. O.; Langkopf, E.; Love, J. A.; Pleuss, N. The First Metal-Catalyzed Intramolecular $[5 + 2]$ Cycloadditions of Vinylcyclopropanes and Alkenes: Scope, Stereochemistry, and Asymmetric Catalysis. *Tetrahedron* **1998**, *54*, 7203–7220.

(30) Wender, P. A.; Dyckman, A. J.; Husfeld, C. O.; Kadereit, D.; Love, J. A.; Rieck, H. Transition Metal-Catalyzed $[5 + 2]$ Cycloadditions with Substituted Cyclopropanes: First Studies of Regio- and Stereoselectivity. *J. Am. Chem. Soc.* **1999**, *121*, 10442–10443.

(31) Wender, P. A.; Williams, T. J. $[(\text{arene})\text{Rh}(\text{cod})]^+$ Complexes as Catalysts for $[5 + 2]$ Cycloaddition Reactions. *Angew. Chem., Int. Ed.* **2002**, *41*, 4550–4553.

(32) Wender, P. A.; Love, J. A.; Williams, T. J. Rhodium-Catalyzed $[5 + 2]$ Cycloaddition Reactions in Water. *Synlett* **2003**, *2003*, 1295–1298.

(33) Wender, P. A.; Haustedt, L. O.; Lim, J.; Love, J. A.; Williams, T. J.; Yoon, J.-Y. Asymmetric Catalysis of the $[5 + 2]$ Cycloaddition Reaction of Vinylcyclopropanes and π -Systems. *J. Am. Chem. Soc.* **2006**, *128*, 6302–6303.

(34) Wender, P. A.; Lesser, A. B.; Sirois, L. E. Rhodium Dinaphthocyclooctatetraene Complexes: Synthesis, Characterization and Catalytic Activity in $[5 + 2]$ Cycloadditions. *Angew. Chem., Int. Ed.* **2012**, *51*, 2736–2740.

(35) Inagaki, F.; Sugikubo, K.; Miyashita, Y.; Mukai, C. Rhodium(I)-Catalyzed Intramolecular $[5 + 2]$ Cycloaddition Reactions of Alkynes and Allenylcyclopropanes: Construction of Bicyclo[5.4.0]-undecatrienes and Bicyclo[5.5.0]dodecatrienes. *Angew. Chem., Int. Ed.* **2010**, *49*, 2206–2210.

(36) Jiao, L.; Yuan, C.; Yu, Z.-X. Tandem Rh(I)-Catalyzed $[(5 + 2) + 1]$ Cycloaddition/Aldol Reaction for the Construction of Linear Triquinane Skeleton: Total Syntheses of (\pm) -Hirsutene and (\pm) -1-Desoxyhypnophilin. *J. Am. Chem. Soc.* **2008**, *130*, 4421–4430.

(37) Fan, X.; Tang, M.-X.; Zhuo, L.-G.; Tu, Y. Q.; Yu, Z.-X. An Expedient and High-Yield Formal Synthesis of Hirsutene using Rh(I)-Catalyzed $[(5 + 2) + 1]$ Cycloaddition. *Tetrahedron Lett.* **2009**, *50*, 155–157.

(38) Fan, X.; Zhuo, L.-G.; Tu, Y. Q.; Yu, Z.-X. Formal Syntheses of (\pm) -Asterisca-3(15),6-diene and (\pm) -Pentalenene using Rh(I)-Catalyzed $[(5 + 2) + 1]$ Cycloaddition. *Tetrahedron* **2009**, *65*, 4709–4713.

(39) Yuan, C.; Jiao, L.; Yu, Z.-X. Formal Total Synthesis of (\pm) -Hirsutic Acid C using the Tandem Rh(I)-Catalyzed $[(5 + 2) + 1]$ Cycloaddition/Aldol Reaction. *Tetrahedron Lett.* **2010**, *51*, 5674–5676.

(40) Liang, Y.; Jiang, X.; Yu, Z.-X. Enantioselective Total Synthesis of $(+)$ -Asteriscanolide via Rh(I)-Catalyzed $[(5 + 2) + 1]$ Reaction. *Chem. Commun.* **2011**, *47*, 6659–6661.

(41) Liang, Y.; Jiang, X.; Fu, X.-F.; Ye, S.; Wang, T.; Yuan, J.; Wang, Y.; Yu, Z.-X. Total Synthesis of $(+)$ -Asteriscanolide: Further Exploration of the Rhodium(I)-Catalyzed $[(5 + 2) + 1]$ Reaction of Ene-Vinylcyclopropanes and CO. *Chem. - Asian J.* **2012**, *7*, 593–604.

(42) Liu, J.; Zhou, Y.; Zhu, J.; Yu, Z.-X. Synthesizing Molecules with Linear Tricyclic 5/5/5 and 6/5/5 Skeletons via $[5 + 2 + 1]$ /Ene Strategy. *Org. Lett.* **2021**, *23*, 7566–7570.

(43) Sameera, W. M. C.; Maseras, F. Transition Metal Catalysis by Density Functional Theory and Density Functional Theory/Molecular Mechanics. *Wiley Interdiscip. Rev.: Comput. Mol. Sci.* **2012**, *2*, 375–385.

(44) Gusev, D. G. Assessing the Accuracy of M06-L Organometallic Thermochemistry. *Organometallics* **2013**, *32*, 4239–4243.

(45) Sperger, T.; Sanhueza, I. A.; Kalvet, I.; Schoenebeck, F. Computational Studies of Synthetically Relevant Homogeneous Organometallic Catalysis Involving Ni, Pd, Ir, and Rh: An Overview of Commonly Employed DFT Methods and Mechanistic Insights. *Chem. Rev.* **2015**, *115*, 9532–9586.

(46) Santoro, S.; Kalek, M.; Huang, G.; Himo, F. Elucidation of Mechanisms and Selectivities of Metal-Catalyzed Reactions using Quantum Chemical Methodology. *Acc. Chem. Res.* **2016**, *49*, 1006–1018.

(47) Dohm, S.; Hansen, A.; Steinmetz, M.; Grimme, S.; Checinski, M. P. Comprehensive Thermochemical Benchmark Set of Realistic Closed-Shell Metal Organic Reactions. *J. Chem. Theory Comput.* **2018**, *14*, 2596–2608.

(48) Ryu, H.; Park, J.; Kim, H. K.; Park, J. Y.; Kim, S.-T.; Baik, M.-H. Pitfalls in Computational Modeling of Chemical Reactions and How to Avoid Them. *Organometallics* **2018**, *37*, 3228–3239.

(49) Vogiatzis, K. D.; Polynski, M. V.; Kirkland, J. K.; Townsend, J.; Hashemi, A.; Liu, C.; Pidko, E. A. Computational Approach to Molecular Catalysis by 3d Transition Metals: Challenges and Opportunities. *Chem. Rev.* **2019**, *119*, 2453–2523.

(50) Funes-Ardoiz, I.; Schoenebeck, F. Established and Emerging Computational Tools to Study Homogeneous Catalysis—From Quantum Mechanics to Machine Learning. *Chem* **2020**, *6*, 1904–1913.

(51) Purvis, G. D., III; Bartlett, R. J. A Full Coupled-Cluster Singles and Doubles Model: The Inclusion of Disconnected Triples. *J. Chem. Phys.* **1982**, *76*, 1910–1918.

(52) Weigend, F.; Ahlrichs, R. Balanced Basis Sets of Split Valence, Triple Zeta Valence and Quadruple Zeta Valence Quality for H to Rn: Design and Assessment of Accuracy. *Phys. Chem. Chem. Phys.* **2005**, *7*, 3297–3305.

(53) Andrae, D.; Häußermann, U.; Dolg, M.; Stoll, H.; Preuß, H. Energy-Adjusted *Ab Initio* Pseudopotentials for the Second and Third Row Transition Elements. *Theor. Chim. Acta* **1990**, *77*, 123–141.

(54) Tao, J.; Perdew, J. P.; Staroverov, V. N.; Scuseria, G. E. Climbing the Density Functional Ladder: Nonempirical Meta-Generalized Gradient Approximation Designed for Molecules and Solids. *Phys. Rev. Lett.* **2003**, *91*, 146401.

(55) Boese, A. D.; Martin, J. M. L. Development of Density Functionals for Thermochemical Kinetics. *J. Chem. Phys.* **2004**, *121*, 3405–3416.

(56) Riplinger, C.; Neese, F. An Efficient and Near Linear Scaling Pair Natural Orbital Based Local Coupled Cluster Method. *J. Chem. Phys.* **2013**, *138*, 034106.

(57) Riplinger, C.; Sandhoefer, B.; Hansen, A.; Neese, F. Natural Triple Excitations in Local Coupled Cluster Calculations with Pair Natural Orbitals. *J. Chem. Phys.* **2013**, *139*, 134101.

(58) Neese, F.; Atanasov, M.; Bistoni, G.; Maganas, D.; Ye, S. Chemistry and Quantum Mechanics in 2019: Give Us Insight and Numbers. *J. Am. Chem. Soc.* **2019**, *141*, 2814–2824.

(59) Burés, J. A Simple Graphical Method to Determine the Order in Catalyst. *Angew. Chem., Int. Ed.* **2016**, *55*, 2028–2031.

(60) Burés, J. Variable Time Normalization Analysis: General Graphical Elucidation of Reaction Orders from Concentration Profiles. *Angew. Chem., Int. Ed.* **2016**, *55*, 16084–16087.

(61) Nielsen, C. D.-T.; Burés, J. Visual Kinetic Analysis. *Chem. Sci.* **2019**, *10*, 348–353.

(62) *Rhodium Catalysis in Organic Synthesis: Methods and Reactions*; Tanaka, K., Ed.; Wiley-VCH: 2019.

(63) Wang, H.; Sawyer, J. R.; Evans, P. A.; Baik, M.-H. Mechanistic Insight into the Diastereoselective Rhodium-Catalyzed Pauson–Khand Reaction: Role of Coordination Number in Stereocontrol. *Angew. Chem., Int. Ed.* **2008**, *47*, 342–345.

- (64) Baik, M.-H.; Mazumder, S.; Ricci, P.; Sawyer, J. R.; Song, Y.-G.; Wang, H.; Evans, P. A. Computationally Designed and Experimentally Confirmed Diastereoselective Rhodium-Catalyzed Pauson–Khand Reaction at Room Temperature. *J. Am. Chem. Soc.* **2011**, *133*, 7621–7623.
- (65) Park, Y.; Ahn, S.; Kang, D.; Baik, M.-H. Mechanism of Rh-Catalyzed Oxidative Cyclizations: Closed versus Open Shell Pathways. *Acc. Chem. Res.* **2016**, *49*, 1263–1270.
- (66) Burrows, L. C.; Jesikiewicz, L. T.; Liu, P.; Brummond, K. M. Mechanism and Origins of Enantioselectivity in the Rh(I)-Catalyzed Pauson–Khand Reaction: Comparison of Bidentate and Monodentate Chiral Ligands. *ACS Catal.* **2021**, *11*, 323–336.
- (67) Wender, P. A.; Barzilay, C. M.; Dyckman, A. J. The First Intermolecular Transition Metal-Catalyzed [5 + 2] Cycloadditions with Simple, Unactivated, Vinylcyclopropanes. *J. Am. Chem. Soc.* **2001**, *123*, 179–180.
- (68) Yu, Z.-X.; Wender, P. A.; Houk, K. N. On the Mechanism of [Rh(CO)₂Cl]₂-Catalyzed Intermolecular (5 + 2) Reactions between Vinylcyclopropanes and Alkynes. *J. Am. Chem. Soc.* **2004**, *126*, 9154–9155.
- (69) Yu, Z.-X.; Cheong, P. H.-Y.; Liu, P.; Legault, C. Y.; Wender, P. A.; Houk, K. N. Origins of Differences in Reactivities of Alkenes, Alkynes, and Allenes in [Rh(CO)₂Cl]₂-Catalyzed (5 + 2) Cycloaddition Reactions with Vinylcyclopropanes. *J. Am. Chem. Soc.* **2008**, *130*, 2378–2379.
- (70) Liu, P.; Cheong, P. H.-Y.; Yu, Z.-X.; Wender, P. A.; Houk, K. N. Substituent Effects, Reactant Preorganization, and Ligand Exchange Control the Reactivity in Rh^I-Catalyzed (5 + 2) Cycloadditions between Vinylcyclopropanes and Alkynes. *Angew. Chem., Int. Ed.* **2008**, *47*, 3939–3941.
- (71) Liu, P.; Sirois, L. E.; Cheong, P. H.-Y.; Yu, Z.-X.; Hartung, I. V.; Rieck, H.; Wender, P. A.; Houk, K. N. Electronic and Steric Control of Regioselectivities in Rh(I)-Catalyzed (5 + 2) Cycloadditions: Experiment and Theory. *J. Am. Chem. Soc.* **2010**, *132*, 10127–10135.
- (72) Xu, X.; Liu, P.; Lesser, A.; Sirois, L. E.; Wender, P. A.; Houk, K. N. Ligand Effects on Rates and Regioselectivities of Rh(I)-Catalyzed (5 + 2) Cycloadditions: A Computational Study of Cyclooctadiene and Dinaphthocyclooctatetraene as Ligands. *J. Am. Chem. Soc.* **2012**, *134*, 11012–11025.
- (73) Hong, X.; Stevens, M. C.; Liu, P.; Wender, P. A.; Houk, K. N. Reactivity and Chemoselectivity of Allenes in Rh(I)-Catalyzed Intermolecular (5 + 2) Cycloadditions with Vinylcyclopropanes: Allene-Mediated Rhodacycle Formation Can Poison Rh(I)-Catalyzed Cycloadditions. *J. Am. Chem. Soc.* **2014**, *136*, 17273–17283.
- (74) Mustard, T. J. L.; Wender, P. A.; Cheong, P. H.-Y. Catalytic Efficiency Is a Function of How Rhodium(I) (5 + 2) Catalysts Accommodate a Conserved Substrate Transition State Geometry: Induced Fit Model for Explaining Transition Metal Catalysis. *ACS Catal.* **2015**, *5*, 1758–1763.
- (75) Liu, C.-H.; Yu, Z.-X. Rhodium(I)-Catalyzed Bridged [5 + 2] Cycloaddition of *cis*-Allene-vinylcyclopropanes to Synthesize the Bicyclo[4.3.1]decane Skeleton. *Angew. Chem., Int. Ed.* **2017**, *56*, 8667–8671.
- (76) Jiao, L.; Lin, M.; Zhuo, L.-G.; Yu, Z.-X. Rh(I)-Catalyzed [(3 + 2) + 1] Cycloaddition of 1-Yne/Ene-vinylcyclopropanes and CO: Homologous Pauson–Khand Reaction and Total Synthesis of (±)-*α*-Agarofuran. *Org. Lett.* **2010**, *12*, 2528–2531.
- (77) Lin, M.; Li, F.; Jiao, L.; Yu, Z.-X. Rh(I)-Catalyzed Formal [5 + 1]/[2 + 2 + 1] Cycloaddition of 1-Yne-vinylcyclopropanes and Two CO Units: One-Step Construction of Multifunctional Angular Tricyclic 5/5/6 Compounds. *J. Am. Chem. Soc.* **2011**, *133*, 1690–1693.
- (78) Wender, P. A.; Gamber, G. G.; Hubbard, R. D.; Pham, S. M.; Zhang, L. Multicomponent Cycloadditions: The Four-Component [5 + 1 + 2 + 1] Cycloaddition of Vinylcyclopropanes, Alkynes, and CO. *J. Am. Chem. Soc.* **2005**, *127*, 2836–2837.
- (79) Mbaezue, I. I.; Ylijoki, K. E. O. [5 + 1 + 2 + 1] vs [5 + 1 + 1 + 2] Rhodium-Catalyzed Cycloaddition Reactions of Vinylcyclopropanes with Terminal Alkynes and Carbon Monoxide: Density Functional Theory Investigations of Convergent Mechanistic Pathways and Reaction Regioselectivity. *Organometallics* **2017**, *36*, 2832–2842.
- (80) Previously, we found that the [5 + 2 + 1] cycloaddition of the standard malonate-tethered substrate was sensitive to the pressure of CO.²³ We propose that its kinetic profile could be similar to that of substrate **1b**.
- (81) The [Rh(CO)₂Cl]₂-catalyzed Pauson–Khand reaction also benefits from a low pressure of CO. See: Kobayashi, T.; Koga, Y.; Narasaka, K. The Rhodium-Catalyzed Pauson–Khand Reaction. *J. Organomet. Chem.* **2001**, *624*, 73–87.
- (82) Kirchhof, M.; Gugeler, K.; Fischer, F. R.; Nowakowski, M.; Bauer, A.; Alvarez-Barcia, S.; Abitaev, K.; Schnierle, M.; Qawasmi, Y.; Frey, W.; Baro, A.; Estes, D. P.; Sottmann, T.; Ringenberg, M. R.; Plietker, B.; Bauer, M.; Kästner, J.; Laschat, S. Experimental and Theoretical Study on the Role of Monomeric vs Dimeric Rhodium Oxazolidinone Norbornadiene Complexes in Catalytic Asymmetric 1,2- and 1,4-Additions. *Organometallics* **2020**, *39*, 3131–3145.
- (83) For each favored alkene insertion transition state, we have performed some preliminary calculations on the subsequent CO insertion. At least one CO insertion transition state is lower than its preceding alkene insertion transition state by 1.9 kcal/mol in terms of Gibbs energy. Therefore, the alkene insertion step is irreversible for these substrates.
- (84) For substrates **1h** and **1i**, preliminary calculations show that at least one C(sp²)–C(sp³) reductive elimination transition state is lower than its preceding CO insertion transition state by 3.6 kcal/mol in terms of Gibbs energy, suggesting that the CO insertion step is irreversible for these substrates.
- (85) Houk, K. N.; Cheong, P. H.-Y. Computational Prediction of Small-Molecule Catalysts. *Nature* **2008**, *455*, 309–313.
- (86) Nguyen, Q. N. N.; Tantillo, D. J. The Many Roles of Quantum Chemical Predictions in Synthetic Organic Chemistry. *Chem. - Asian J.* **2014**, *9*, 674–680.
- (87) Sperger, T.; Sanhueza, I. A.; Schoenebeck, F. Computation and Experiment: A Powerful Combination to Understand and Predict Reactivities. *Acc. Chem. Res.* **2016**, *49*, 1311–1319.
- (88) Bo, C.; Maseras, F.; López, N. The Role of Computational Results Databases in Accelerating the Discovery of Catalysts. *Nat. Catal.* **2018**, *1*, 809–810.
- (89) Ahn, S.; Hong, M.; Sundararajan, M.; Ess, D. H.; Baik, M.-H. Design and Optimization of Catalysts Based on Mechanistic Insights Derived from Quantum Chemical Reaction Modeling. *Chem. Rev.* **2019**, *119*, 6509–6560.
- (90) For instance, on the basis of our mechanistic insights, one may use quantum chemical calculations to predict whether a known [*m* + *n*] cycloaddition can be developed into an unprecedented [*m* + *n* + *o*] cycloaddition and in which step the new component (e.g., CO) will be embedded.
- (91) Frisch, M. J.; Trucks, G. W.; Schlegel, H. B.; Scuseria, G. E.; Robb, M. A.; Cheeseman, J. R.; Scalmani, G.; Barone, V.; Mennucci, B.; Petersson, G. A.; Nakatsuji, H.; Caricato, M.; Li, X.; Hratchian, H. P.; Izmaylov, A. F.; Bloino, J.; Zheng, G.; Sonnenberg, J. L.; Hada, M.; Ehara, M.; Toyota, K.; Fukuda, R.; Hasegawa, J.; Ishida, M.; Nakajima, T.; Honda, Y.; Kitao, O.; Nakai, H.; Vreven, T.; Montgomery, J. A., Jr; Peralta, J. E.; Ogliaro, F.; Bearpark, M.; Heyd, J. J.; Brothers, E.; Kudin, K. N.; Staroverov, V. N.; Keith, T.; Kobayashi, R.; Normand, J.; Raghavachari, K.; Rendell, A.; Burant, J. C.; Iyengar, S. S.; Tomasi, J.; Cossi, M.; Rega, N.; Millam, J. M.; Klene, M.; Knox, J. E.; Cross, J. B.; Bakken, V.; Adamo, C.; Jaramillo, J.; Gomperts, R.; Stratmann, R. E.; Yazyev, O.; Austin, A. J.; Cammi, R.; Pomelli, C.; Ochterski, J. W.; Martin, R. L.; Morokuma, K.; Zakrzewski, V. G.; Voith, G. A.; Salvador, P.; Dannenberg, J. J.; Dapprich, S.; Daniels, A. D.; Farkas, Ö.; Foresman, J. B.; Ortiz, J. V.; Cioslowski, J.; Fox, D. J. *Gaussian 09, Rev. E.01*; Gaussian, Inc.: 2013.
- (92) Zhao, Y.; Truhlar, D. G. Computational Characterization and Modeling of Buckyball Tweezers: Density Functional Study of Concave–Convex $\pi\cdots\pi$ Interactions. *Phys. Chem. Chem. Phys.* **2008**, *10*, 2813–2818.

(93) Ribeiro, R. F.; Marenich, A. V.; Cramer, C. J.; Truhlar, D. G. Use of Solution-Phase Vibrational Frequencies in Continuum Models for the Free Energy of Solvation. *J. Phys. Chem. B* **2011**, *115*, 14556–14562.

(94) Marenich, A. V.; Cramer, C. J.; Truhlar, D. G. Universal Solvation Model Based on Solute Electron Density and on a Continuum Model of the Solvent Defined by the Bulk Dielectric Constant and Atomic Surface Tensions. *J. Phys. Chem. B* **2009**, *113*, 6378–6396.

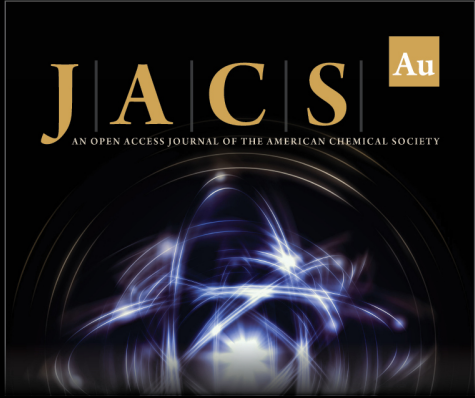
(95) Neese, F. The ORCA Program System. *Wiley Interdiscip. Rev.: Comput. Mol. Sci.* **2012**, *2*, 73–78.

(96) Neese, F. Software Update: The ORCA Program System, Version 4.0. *Wiley Interdiscip. Rev.: Comput. Mol. Sci.* **2018**, *8*, No. e1327.


(97) Veleckis, E.; Hacker, D. S. Solubility of Carbon Monoxide in 1,4-Dioxane. *J. Chem. Eng. Data* **1984**, *29*, 36–39.


(98) Keith, J. A.; Carter, E. A. Quantum Chemical Benchmarking, Validation, and Prediction of Acidity Constants for Substituted Pyridinium Ions and Pyridinyl Radicals. *J. Chem. Theory Comput.* **2012**, *8*, 3187–3206.


(99) Legault, C. Y. *CYLview, 1.0b*; Université de Sherbrooke: 2009; <http://www.cylview.org> (accessed 2017-10-07).



JACS Au
AN OPEN ACCESS JOURNAL OF THE AMERICAN CHEMICAL SOCIETY

 Editor-in-Chief
Prof. Christopher W. Jones
Georgia Institute of Technology, USA

Open for Submissions 

pubs.acs.org/jacsau  ACS Publications
Most Trusted. Most Cited. Most Read.